A POLARIMETRIC HYPERSPECTRAL IMAGING SENSOR

Li-Jen Cheng

Jet Propulsion Laboratory
California Institute of Technology
Pasadena, California 91109

ABSTRACT

This paper reports recent field test results of a polarimetric hyperspectral imaging prototype sensor using a noncollinear acousto-optic tunable filter as a wavelength sorter and a polarizing beam splitter. The objective of this work is to evaluate the AOTF-PHI technology for a variety of remote sensing applications.

INTRODUCTION

Acousto-optic tunable filter (AOTF) is a high resolution, rapidly tunable spectral bandpass filter that uses the diffraction of an incident light beam at a moving grating produced by an acoustic wave in a birefringent crystal,' This device has a large aperture and is suitable for imaging applications, The selection of operating wavelength is done by tuning the frequency of a RF power supply connected to a transducer mounted on the crystal, Therefore, the filter can be operated in a sequential, random (wavelength hopping), or multiple wavelength mode with a wavelength switching time in the order of 10 μsec, providing an operational flexibility, Furthermore, AOTFS can provide high spectral resolution ($\lambda/\Delta\lambda$) of 10^2-10^4 This high resolution capability gives opportunities to characterize materials through the remote sensing of reflection, absorption, or emission spectrum. With proper optics and focal plane arrays, one can develops a polarimetric hyperspectral imaging (PHI) sensor capable of providing two spectral image cubes of polarization orthogonally to each other.

In the past, we developed two AOTF-PHI breadboard systems using TeO_2 AOTFs, one operating in the 0,48-0.76 μm range and the other in the range of 1.2 to 2.5 μm. Their performance was investigated in the laboratory environment.[2,3] A visible/near-infrared PHI prototype sensor using a Te02 AOTF was recently developed[4] and tested in outdoor field experiments.[5] The sensor was put together with the out-of-the-shelf items. Therefore, its

performance is far from the ideal, However, it is capable to provide needed information for illustrating the potential of the AOTF technology for remote sensing applications,

OIISERVATIONS

Figure 1 gives a grayscale image of the test scene in Ft. Huachuca, AZ that was taken with an ordinary 35 mm camera, The scene contained a variety oft ypical southern Arizona plants and a small number of Army exercise facilities. There were mesquites at the bottom of the image, Above mesquites, there were groups of trees with open areas among them, Some trees were oaks. Beyond the tree-rich region, there was a wide open area with reddish soil, dry grass, a dirt road, bushes, yuccas, and two trees, In the top part of the scene, there were cascaded ridges with a mixture of green trees and yellow dry grass, Some Army facilities and tents were located in the area at the boundary of the tree-rich area and the open area. They included a disk antenna and a pole antenna. The boundary was about 3.1 km away from the instrument. In addition, there was a reflection reference plate of $BaSO_4$ observable as a small bright rectangular object in the upper left part of the picture, that was used for intensity normalization, The distance between the plate and the instrument was about 3.6 km, The observation was carried at the noon time of a sunny day in the spring of 1993, The atmosphere was clear with observable haze only when one looked at distant objects. The instrument directed at the north with 12 degrees off to east,

RESULTS

Vegetation Signatures

Figure 2 gives a spectral image of the scene at 0.67 μm at which the chlorophyll absorption is at maximum, Consequently, oak trees appeared to be dark, whereas mesquites were in gray. In general, all dark and gray areas were related to vegetation. The bright areas contained mainly dry grass. Figure 3 gives reflected intensity spectra of oak and mesquite located in the lower left part of the scene, illustrating that the reflectance of oak is considerably lower than that of mesquite in the 0.62-0.69 μm wavelength range, consistent with the observed image.

The observed spectra also show a sharp rise in reflectance between 0.69 and 0,73 pm, known as the "red edge". The slope and position of the red edge have been directly correlated with leaf chlorophyll concentration.[6] The sharp rise provides an effective way to map veget at ion using spectral derivatives. Figure 4 gives a spectral derivative image of the scene at 0.71 μm. Bare ground and dry grass are often bright objects in the intensity image, However, they often do not have chlorophyll, So, their reflection does not have a strong spectral dependence in this wavelength range. Consequently, they are dark in the spectral derivative image, The brightness in the image relates to leaf chlorophyll concentration. Therefore, the spectral derivative image is an effective approach for monitoring health state and stress response in vegetation,

Aerosol Scattering Effects

The existence of atmospheric boundary-layer aerosols affects the magnitude, shape, and polarization of the spectra. The effects become substantial in the observation of distant objects. The measured differences in intensity, spectrum, and polarization due to the

distance can provide important information about the aerosol. Using spectral and polarization data of two oak trees located at different distances from the instrument, we obtained the wavelength dependence of the scattering in the air at the observation sites

In general, the scattered light spectrum due to the molecules and aerosol in the atmosphere is expected to a negative wavelength power dependence.' Therefore, we obtained a smooth inverted wavelength power function from the observed spectra using an iterative approach. Figure 5 gives the observation data with fitting descending curves of $200.7\lambda^{-2.043}$ for vertical polarization and $56.4\ \lambda^{-2.48}$ for horizontal polarization, where λ is the wavelength. The obtained λ dependence is consistent with the clear atmosphere of the day.'

Polarization Signatures

Polarization is an important parameter for analyzing signatures of objects obtained from a remote sensing instrument. Each AOTF observation creates two spectral image cubes with polarization orthogonal to each other. The data reported here are differential polarization defined as the difference in intensity at one corresponding pixel of the two polarization images divided by the sum of the intensities,

Figure 6 gives measured polarization spectra of oak, mesquite, and a unknown tree for illustrating some interesting spectral polarization features of tree leaves. It should be noted that the measured spectrum contains two components. One is due to the polarization created by various scattering mechanisms in the atmosphere. This scattering component is a monotonically decreasing smooth function of wavelength as illustrated in Figure 5. Therefore any significant structure observed in the polarization spectra shall relates to the object property.

Canopies have polarization signatures.[8-10] The spectral dependence of the signatures has not been studies extensively. The data in Figure 6 have revealed that leaves of these trees have a similar polarization spectral signature, namely a sharp descending step at 0,69 μm beyond which the signal is low. The observation suggests that the sharp decreasing feature could be related to the red edge,

Figure 7 gives a spectral polarization image at 0.56 μm. The image illustrates two important observations, All the vegetation have polarization signatures and the measured polarization signal increases with distance, The latter is due to aerosol scattering . This component increases with the observation distance.

Object Detection

There were several military facilities in the boundary area between the tree and open areas. Here we reported only the detection of a camouflaged target located near the center of the scene. We located the target as a dark pattern near the middle of the polarization images at wavelengths around 0,56 μm as shown in Figure 7. Figure 8 gives enlarged positive and negative images. The target pattern also appeared in the secondary spectral derivative images in the same wavelength range. The target was composed of several different objects, Each object has its own spectral dependence. Around 0.56 μm, they appeared together as the observed pattern.

In the color image, the lower part of the target appeared to be bright green trees with two separated green spherical objects. In the polarization picture, the spherical objects were very dark dots with a dark line between them forming a dumbbell pattern, The dumbbell pattern is likely to be a man-made object. In addition, in the polarization picture, the image of the 'green tree' area was composed with several broad horizontal gray line segments arranged in the shape of an inverted acute triangle.

These contradicting observations between the color and spectral polarization images, we concluded that we detected a camouflaged target area, A detailed observation at the enlarged picture provided a verification that the 'green tree' was green camouflage nets covering unknown objects and neighboring tree tops, The detection was mainly due to the spectral polarization imaging capability of the AOTF-PH1 system, It ought to note that the lower part of the pattern was also observable in spectral images of green wavelengths, However, the spectral polarization data provided the evidence for the determination of the target being camouflaged.,

CONCLUSION

Our field test results have illustrated the powerful capability of the AOTF-PHI technology for a variety of remote sensing applications, including object detection in the different surroundings, The results also show the complexity of the outdoor environment, In order to take the advantages of PHI, there is a need to understand the fundamental physical phenomena related to the observation and to establish data bases of object signatures and environmental influences.

ACKNOWLEDGMENT

The research described in this paper was performed by the Center for Space Microelectronics Technology, Jet Propulsion Laboratory, California Institute of Technology, and was jointly sponsored by the National Aeronautics and Space Administration, the Planetary Instrument Definition and Development Program, and the Army Space Technology and Research Office.

REFERENCES

1. I.C. Change, "Noncollinear Acousto-Optic Filter with Large Angle Aperture", Appl. Phys. Lett., Vol. 25, p.370 (1974).

2. Tien-Hsin Chao, Jeffrey Yu, George Rcycs, David Rider and Li-Jen Cheng, "Acousto-Optic Tunable Imaging Spectrometers", Proceedings of 1991 International Geoscience and Remote Sensing Symposium, Helsinki, Espoo, FINLAND, June, 1991 (IEEE 91CH2971-O), p. 585.

3. Li-Jen Cheng, Tien-Hsin Chao, and George Reycs, "Acousto-Optic Tunable Filter Multispectral Imaging System", AIAA Space Programs and Technologies Conference, March 24-27, 1992, paper no, 92-1439,

4. Li-Jen Cheng, Tien-Hsin Chao, Mack Dowdy, Clayton LaBar, Colin Mahoney, George Reyes, and Ken Bergman, " Multispectral Imaging Systems Using Acousto-Optic Tunable Filter" , in "Infrared and Millimeter Wave Engineering" , SPIE Proceedings Vol. 1874, p. 224 (1993),

5. Li-Jen Cheng, Mike Hamilton, Colin Mahoney, and Georgre Reycs, "Analysis of AOTF hyperspectral Imagery", To be published in "Algorithms for Multispectral and Hyperspectral Imagery", SPIE Proceedings, Vol. 2231, 1994,

6. For example, D.N.H. Horler, M. Dockray, J. Barber, and A.R. Baringer, "Red Edge Measurements for Remotely Sensing Plant Chlorophyll Contents", Adv. Space Res. 3(2), 273 (1983).

7. E. Schanda, "Physical Fundamentals of Remote Sensing", (Sringer-Verlog, New York, 1986), p.117.

8. P. J. Curran, "The Relationship Between Polarized Visible Light and Vegetation Amount", Remote Sens. Environ., Vol. 11, p. 87 (1981),

9. D.A. Talmage and P.J. Curran, "Remote Sensing Using Partially Polarized Light", Int. J. Remote Sensing, Vol.7, p.47, (1986).

10. V. V. Vanderbilt and L.J. De Venecia, "Specular, Diffuse, and Polarized Imagery of an Oat Canopy", IEEE Trans. Geosci. Remote Sensing, Vol.26, p.451 (1988).

Figure 1. Grayscale image of the scene,

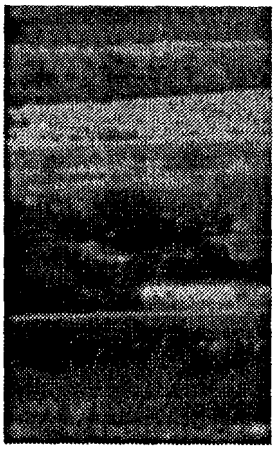

Figure 2, Spectral image at 0,63 μm.

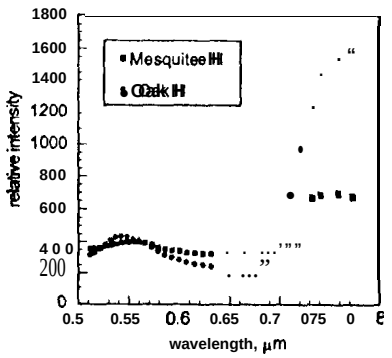

Figure 3. Reflectance spectra of oak and mesquite with horizontal polarization

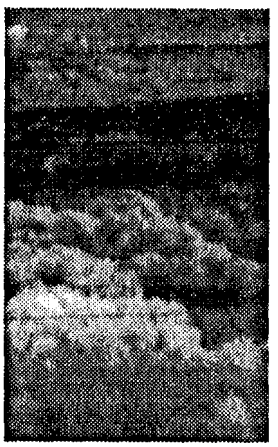

Figure 4. Spectral derivative image at 0.71 μm.

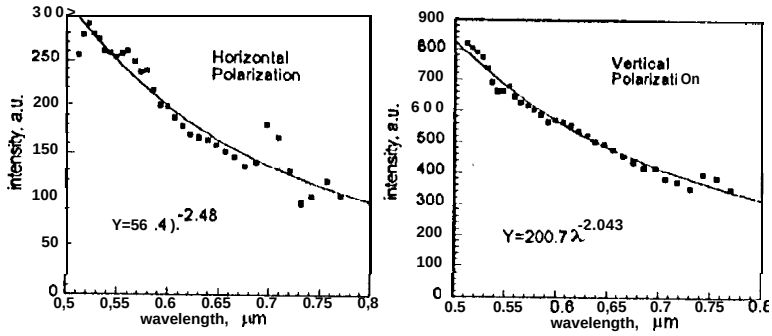

Figure 5. Estimated aerosol-rclaied components of the observed spectra for horizontal and vertical polarization,

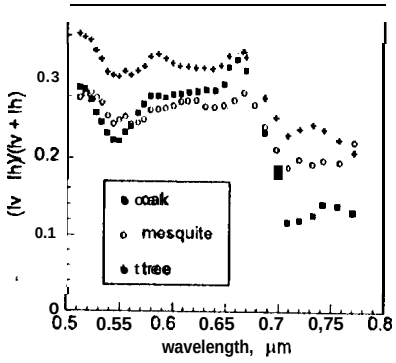

Figure 6. Polarizationspectra of oak, mesquite, and unknown tree,

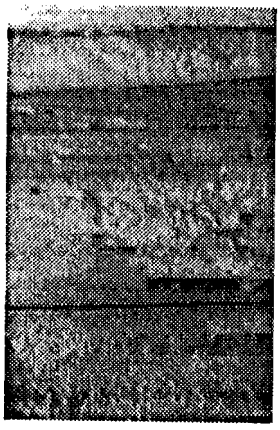

Figure 7. Spectral polariization image at 0,56 pm,

Figure 8. Enlarged positive (upper) and negative (lower) images of the target area.